Korean J. Chem. Eng., **29**(11), 1541-1548 (2012)
DOI: 10.1007/s11814-012-0037-9

Characterizations of impedance responses in an anode-supported solid oxide fuel cell with an air blowing system

Ju Hee Kim*, Young Min Park, and Haekyoung Kim*,†**

*School of Materials Science & Engineering, Yeungnam University, Gyeongsan 712-749, Korea
**Fuel Cell Project, Research Institute of Industrial Science and Technology, Pohang 790-330, Korea
(*Received 18 December 2011 • accepted 14 March 2012*)

Abstract−Effects of operation parameters on impedance responses are characterized to study electrochemical reactions of an anode-supported solid oxide fuel cell (SOFC) in an air blowing operation. The anode-supported SOFC, which consists of Ni-yttrium stabilized zirconia (YSZ) support/Ni-YSZ anode functional layer/YSZ electrolyte/gadolinium doped ceria (GDC) interlayer/$La_{0.6}Sr_{0.4}Co_{0.2}Fe_{0.8}O_{3-\delta}$-GDC cathode, is fabricated by a tape casting and co-firing process. To investigate the electrochemical response on impedances, an equivalent circuit is modeled with five elements and fitted by the complex nonlinear least square (CNLS) method. Based on the impedance spectra with the operation parameters, two among five elements are clarified to be concerned with anodic reactions and another two concerned with gas diffusion reactions in electrodes. It is difficult to clarify one among five elements with the results here. The clarified elements may be used to study the effects of materials and processes for SOFC with impedance responses, which will be helpful to improve the performance and reliability.

Key words: Solid Oxide Fuel Cell, Impedance Spectra, Anode-supported Cell, Equivalent Circuit, Air Blowing

INTRODUCTION

Fuel cells, which convert chemical energy such as hydrogen, methanol, ethanol, formic acid, and methane, into electric energy, have several potential advantages over direct combustion devices, including higher efficiency, lower/zero emissions, and higher power density. Although more than seven types of fuel cells have appeared, solid oxide fuel cells (SOFCs) are believed to be the most promising future component of energy generation systems [1-3]. Their high-temperature operation above 700 ºC accelerates electrochemical oxidation of fuel with non-precious materials and produces high-quality heat as a byproduct for cogeneration. The development of low-cost materials and fabrication processes is the key technical challenge facing SOFCs [4-6]. The anode-supported design for SOFCs has been extensively investigated due to its ease of fabrication, robustness, and high electrochemical performance [7-11]. The parameters, such as composition and thickness of an anode functional layer [12-15], cathode materials, and GDC interlayer [16-21], have been studied for anode-supported SOFCs. For the state-of-the-art in anode-supported SOFCs (ASCs) operating at 700-800 ºC, the anode - supported SOFC consists of Ni-YSZ support, Ni-YSZ anode functional layer, YSZ electrolyte, Gd-doped ceria (GDC)-based interlayer, and $La_{0.6}Sr_{0.4}Co_{0.2}Fe_{0.8}O_{3-\delta}$ (LSCF) - GDC composite cathode [22-31].

Several electrochemical reactions, such as charge transfer at electrodes, gas-coupled reactions, and gas diffusion reactions, occur in anode-supported SOFCs, and those reactions are concerned with the parameters such as the properties of materials, processes for fabrications, operation conditions, etc [32-34]. To characterize the correlations between the parameters (materials properties, processes, operation conditions, etc.) and fuel cell performance, one of the most important and promising methods is electrochemical impedance spectroscopy (EIS). Electrochemical impedances are the overlapped spectra from several electrochemical reactions in response to AC voltage perturbation, and the vague nature of the impedance responses makes it difficult to break the measured impedance values down into the corresponding electrochemical reactions. EIS has been widely used for performance evaluation and degradation diagnosis, and is helpful to improve and optimize the fuel cell performance. However, recently, many researchers have proposed electrochemical equivalent circuit models (ECM) in order to investigate the electrochemical reactions for ASCs, and the proposed ECMs are well matched with their experimental data [32-38]. Schichlein introduced the distribution of relaxation time (DRT) method to deconvolute the electrochemical impedance spectra of SOFCs [38]. Schichlein suggested that the measured data from EIS are overlapped spectra with each electrochemical reaction, which has a different relaxation time constant. An equivalent circuit model composed of five RQ (resistance and constant phase element) impedance elements connected in series (an inductor, resistor, and five elements) was also suggested [33-39]. With the help of proper impedance models, mass diffusion and charge transfer contributions to the whole polarization can be isolated [40-42].

The aim of this paper is to identify contributions of cell components on the cell resistance to accelerate SOFC commercialization. To understand and improve fuel cell performance with electrochemical reactions, in this study, the current-voltage characteristics and impedances of an anode-supported SOFC in an air blowing system are measured and characterized with various conditions, including flow rate, temperature, partial pressure, air blowing rate, and so on. The impedances of SOFC are characterized by a complex nonlinear least square (CNLS) fitting with the equivalent circuit devel-

†To whom correspondence should be addressed.
E-mail: hkkim@ynu.ac.kr

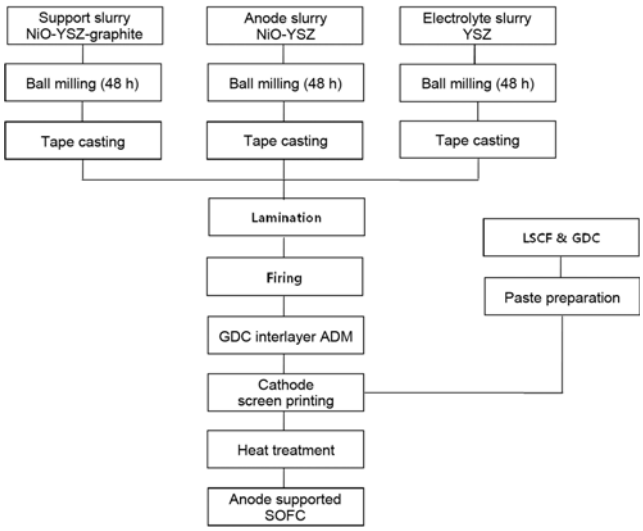

Fig. 1. Process for fabrication of Anode supported SOFC.

oped with five RQ in series. The fitted results are compared with the measured data, and the five elements are studied to clarify electrochemical events by varying operation parameters. To investigate the parameter dependence of each single polarization process, a series of impedance measurements is carried out in which only one cell parameter at a time is varied.

EXPERIMENTAL PROCEDURES

The anode-supported SOFC was fabricated by a co-firing process with three thin layers of support, anode and electrolyte as shown in Fig. 1. The slurry for porous support consisted of NiO (0.4 μm, Kojundo Chemical Lab., Japan), 8 mol% Y_2O_3-stabilized ZrO_2 (YSZ, TZ8Y, Tosoh, Japan), graphite as a pore former (Carbonix, Korea), and binder. The starting materials were mixed and ball-milled with zirconia balls (diameter=10 mm and 5 mm) for 48 h. To prepare the anode functional layer, NiO and YSZ powders in a 6 : 4 weight ratio were mixed and ball milled with binder and solvent. The YSZ electrolyte tape was prepared with YSZ powder and binder. The support, anode, and electrolyte tape layers were laminated with 40 MPa at 80 °C for 10 min. The laminated tapes, consisting of an NiO-YSZ support layer, an NiO-YSZ anode functional layer (AFL), and a YSZ electrolyte, were 25 cm×25 cm. They were co-fired at 700 °C for 2 h to burn out the binder, organic additives, and pore formers. Subsequently, the laminated tapes were sintered at 1,370 °C for 3 h. The GDC interlayer of ~1 μm was formed on YSZ electrolyte via an aerosol deposition method. The anode-supported cells, Ni-YSZ support (~900 μm)/Ni-YSZ AFL (~15 μm)/YSZ (~10 μm)/GDC, were cut by water jet method into circles with diameters of 2.6 cm from a sintered plate. A composite paste with $La_{0.6}Sr_{0.4}Co_{0.2}Fe_{0.8}O_{3-\delta}$ (LSCF, Seimi Chemicals, Japan) and GDC (Anan Kasei, Japan) in a 6 : 4 weight ratio as a cathode electrode was screen printed on the GDC interlayer of the co-fired cell. Subsequently, a paste with LSCF was screen printed on the LSCF - GDC composite cathode to improve the current collection. The cathode active area was 1 cm^2. The fabricated cell was assembled and sealed with Cerama bond™ 571 from AREMCO to measure the current-voltage characteristics and impedances in an alumina jig. The Pt paste and mesh were used for current collecting. The cell was heated to 800 °C in 9 h, and anode reduction was performed with 200 $ccmin^{-1}$ of 97% H_2 - 3% H_2O for 3 h. The current-voltage characteristics of the anode-supported SOFC were tested with 200 $ccmin^{-1}$ of 97% H_2 - 3% H_2O and 1,000 $ccmin^{-1}$ of air at 800 °C, 750 °C, and 700 °C with electronic load of KIKUSUI PLZ-30F. After obtaining the electrochemical performance at 700 °C, the cells were reheated to 750 °C. The impedances of the SOFC were measured at the over-potential from 0 to 0.7 V. To study the effects of fuel and oxidant on the anode and cathode electrode, the flow rate of H_2 was varied from 50 to 300 $ccmin^{-1}$ and the flow rate of blowing air was controlled from 250 to 2,000 $ccmin^{-1}$. The effects of the H_2 and O_2 partial pressure on impedance spectra were also characterized. The impedance measurements were carried out with a Biologic SP300 in the frequency range from 100 kHz to 0.1 Hz with applied AC voltage amplitude of 100 mV. After electrochemical measurements were taken, the microstructures of the SOFC were characterized via scanning electron microscopy using a JSM-6480LV.

RESULTS AND DISCUSSION

The cross-sectional images of anode-supported SOFCs are shown in Fig. 2, and a good adhesion between all layers is observed. ASC consists of a ~900 μm NiO-YSZ support layer, a 15 μm NiO-YSZ

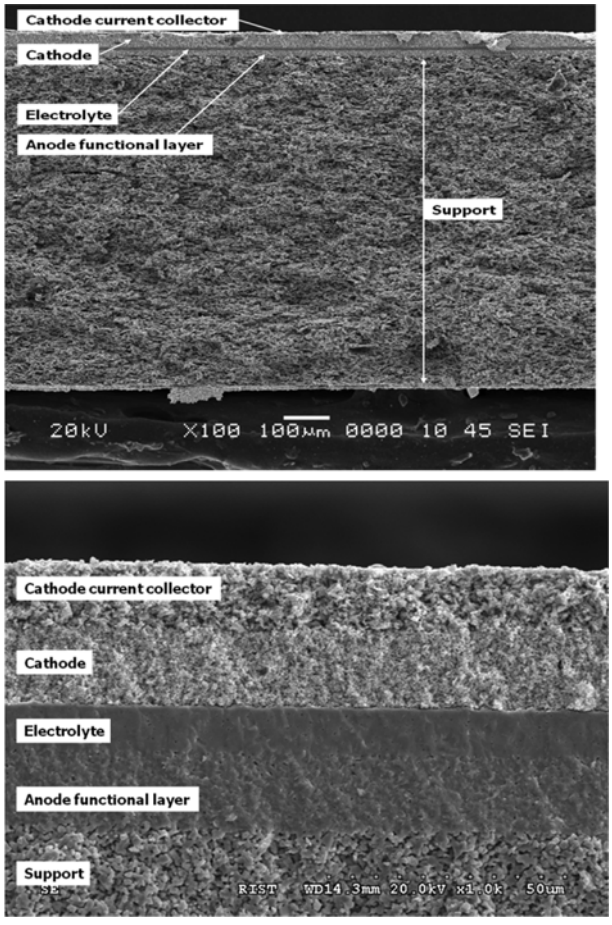

Fig. 2. Cross-sectional Image of anode supported SOFC.

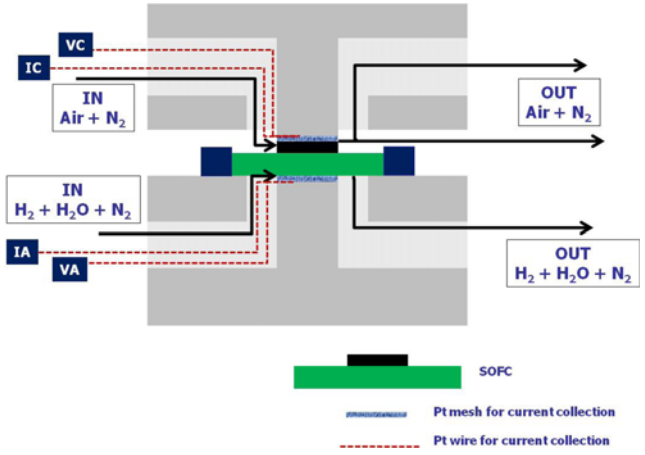

Fig. 3. Schematic diagram of a measuring jig.

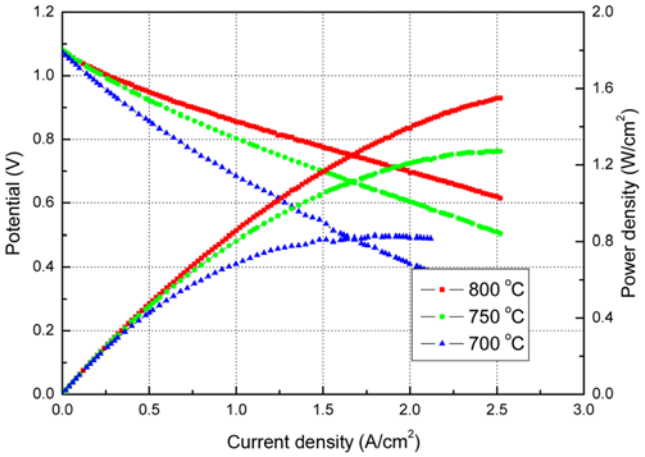

Fig. 4. Current-voltage characteristics of the anode supported SOFC.

layer as an anode functional layer (AFL), a ~10 μm YSZ electrolyte, a GDC interlayer, and a cathode layer. The schematic diagram of a measurement jig for air blowing system is shown in Fig. 3. An anode fuel flows parallel with the anode support and is diffused vertically into a porous anode support and an anode functional layer. The air is supplied as a blowing type.

The power densities of the ASC at 0.9 V are 0.68 Wcm^{-2}, 0.51 Wcm^{-2}, and 0.34 Wcm^{-2} at 800 °C, 750 °C, and 700 °C, respectively, as shown in Fig. 4. The fuel cell performance is good enough to study impedance analysis. The impedance spectra as a function of over-potential from 0 V to 0.7 V at 750 °C are shown in Fig. 5. The impedance values decrease and re-increase with increasing over-potential as shown in Fig. 5(a). The high frequency intercept of impedance spectra represents the ohmic resistance of ASC. The low frequency intercept of impedance spectra shows the area specific resistance (ASR) of the SOFC, and the slope of the current-voltage curve at each potential is identical to the ASR measured by impedance measurements. At near open circuit voltage, the activation polarization is dominant, and the contribution of activation polarization decreases with increasing over-potential. Therefore, the ASR value at the high over-potential is much lower than that at open circuit voltage. As shown in Fig. 4, the decrease of the slope in the current-

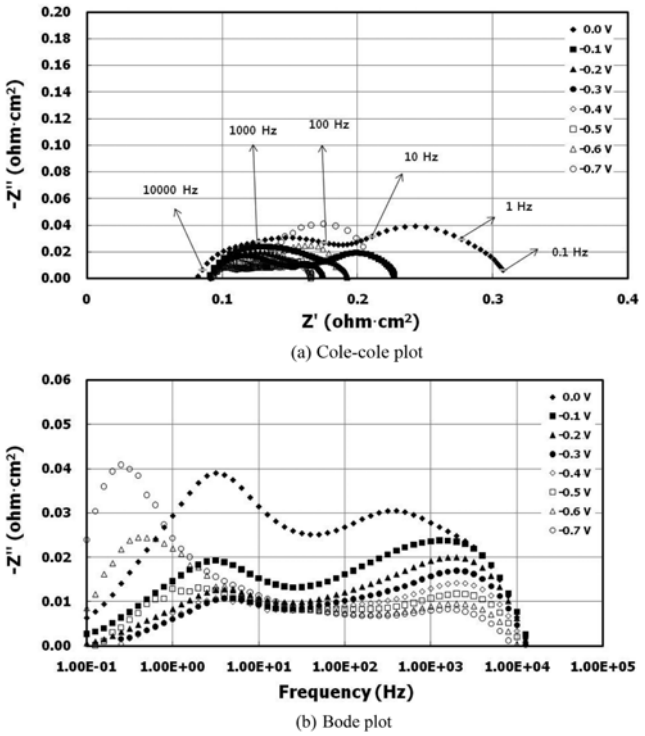

Fig. 5. Impedance spectra as a function of over-potential (0-0.7 V). (a) Cole-cole plot, (b) Bode plot.

voltage curve is observed with the over-potential ranging from 0 V to 0.4 V. However, with increase of the over-potential from 0.5 V to 0.7 V, the ASRs increase. When the impedance is plotted with a frequency in Fig. 5(b), the semi-circle at high frequency range (100-1,000 Hz) decreases with increasing over-potential. However, the semi-circle at low frequency range (0.1-10 Hz) decreases with increase of the over-potential from 0 V to 0.4 V, and it re-increases with increase of the over-potential from 0.5 V to 0.7 V. This phenomenon shows that the mass transfer polarization is decreased and re-increased with over-potential [39], which means that the mass transfer limit exhibits at over-potential higher than 0.5 V in this study.

The impedance spectra with H_2 flow rate at OCV are shown in Fig. 6(a) and (b). The low frequency intercepts (ASRs) with various H_2 flow rate exhibit similar values as shown in Fig. 6(a). However, the different overlapped impedance spectra are observed in a Bode plot of Fig. 6(b). With the higher H_2 flow rate, the charge transfer and gas diffusion reaction might be enhanced, which results in lowered impedance. However, here, H_2 flow rate in the range of 30 to 200 $ccmin^{-1}$ is ineffective on the total impedances. Even though ASRs exhibit similar values, the impedances show the different responses with frequencies. With a higher H_2 flow rate over 150 $ccmin^{-1}$, two vertexes are observed at ~1,000 Hz and 1-10 Hz. With a lower H_2 flow rate of less than 100 $ccmin^{-1}$, three vertexes are observed at ~1,000 Hz, 1-10 Hz, and ~0.1 Hz. It shows that with decreasing H_2 flow rate, the overlapped spectra can be clearly separated. The impedances with the H_2 flow rate can be helpful to distinguish the physical events, which correlate that the charge transfer, charge transfer coupled with gas diffusion, and mass transfer.

By controlling the amount of H_2 and N_2, the partial pressure of H_2 was controlled. The flow rate of mixed fuel was maintained at

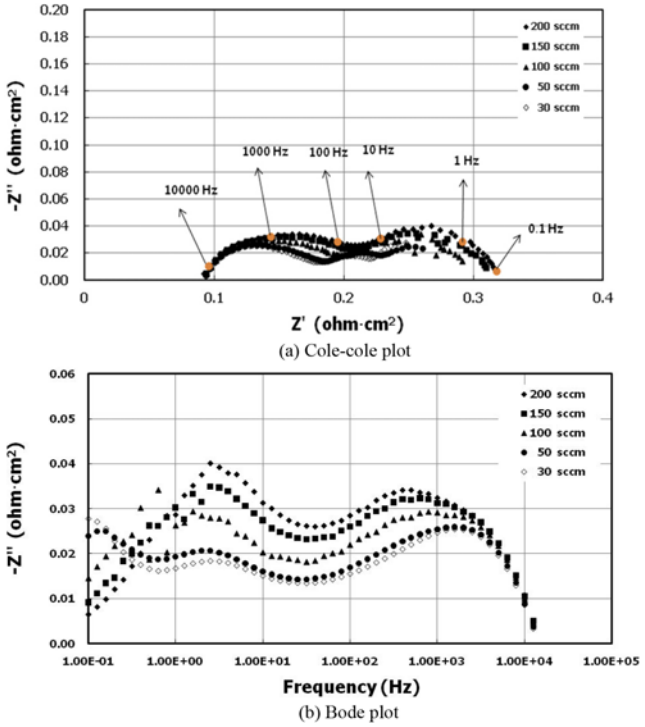

Fig. 6. Impedance spectra as a function of H_2 flow rate (200, 150, 100, 50, and 30 ccmin^{-1}). (a) Cole-cole plot, (b) Bode plot.

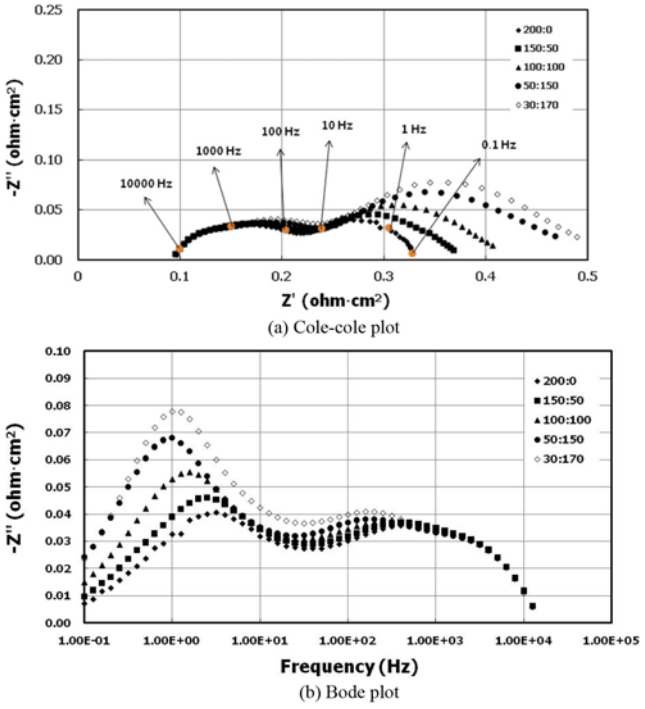

Fig. 7. Impedance spectra as a function of H_2 and N_2 ratio (200 : 0, 150 : 50, 100 : 100, 50 : 150, and 30 : 170 ccmin^{-1}). (a) Cole-cole plot, (b) Bode plot.

200 ccmin^{-1}, and the ratio of H_2 to (H_2+N_2) was varied. The impedances are with the partial pressure of H_2 at OCV shown in Fig. 7. As shown in Fig. 7(b), the imaginary part at the high frequency range of 100-1,000 Hz has similar values, and those at the low frequency

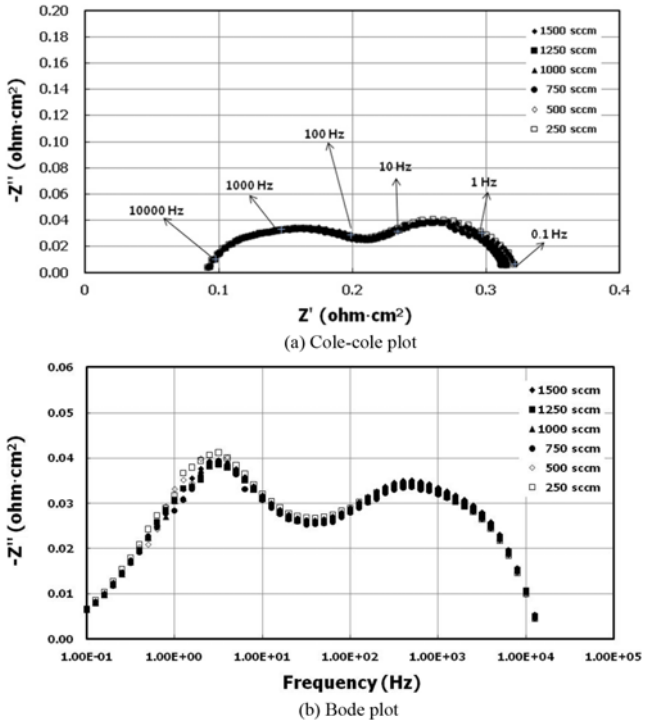

Fig. 8. Impedance spectra as a function of Air flow rate (1,500, 1,250, 1,000, 750, 500, and 250 ccmin^{-1}). (a) Cole-cole plot, (b) Bode plot.

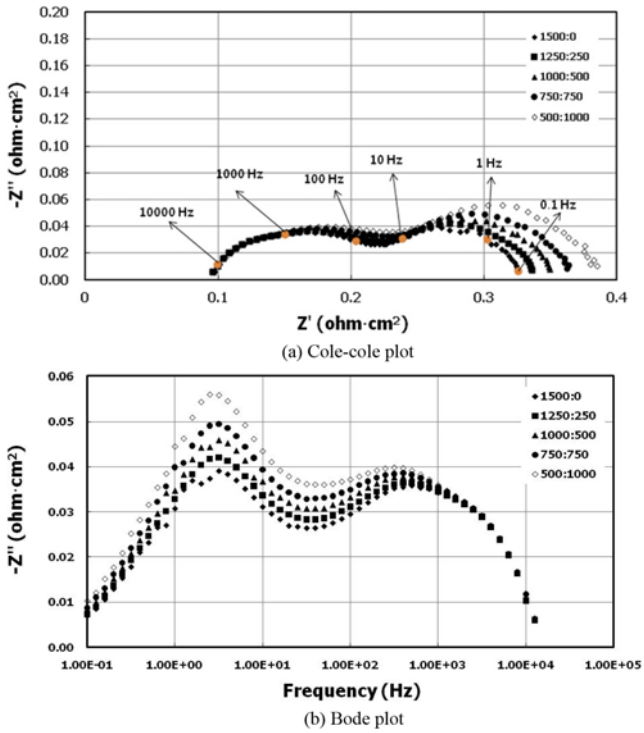

Fig. 9. Impedance spectra as a function of Air and N_2 ratio (1,500 : 0, 1,250 : 250, 1,000 : 500, 750 : 750, and 500 : 1,000 ccmin^{-1}). (a) Cole-cole plot, (b) Bode plot.

range of −1 Hz increase with decreasing H_2 partial pressure. This might mean that the polarization increases at lower H_2 partial pres-

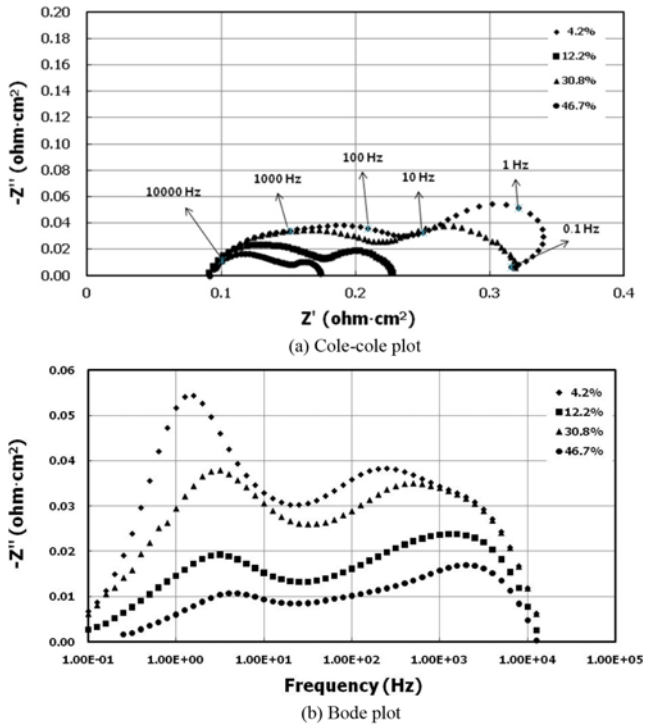

Fig. 10. Impedance spectra as a function of P_{H_2O} (4.2%, 12.2%, 30.8%, and 46.6%). (a) Cole-cole plot, (b) Bode plot.

sure due to the fuel gas diffusion into the AFL, which needs to be further studied with varying the parameters. Figs. 8 and 9 show the impedance spectra at OCV with air flow rate and oxygen partial pressure. The air flow rate has no effect on the impedance spectra. However, the increment of the O_2 partial pressure reduces the impedance value of the ASC. With increasing H_2O partial pressure, the impedance values at OCV decrease as shown in Fig. 10. The imaginary parts at both frequency ranges of 100-1,000 Hz and 1-10 Hz decrease with increasing H_2O partial pressure. The H_2O partial pressure might affect the charge transfer polarization at the high frequency range and the mass transfer polarization at the low frequency range. With the results with various operation conditions in the air blowing system, the anode-supported SOFC shows the increment in fuel cell performance with increasing partial pressure of H_2, O_2, and H_2O. The air flow rate has no effect on the impedance at open circuit voltage and 750 °C. The total impedance is not changed with the H_2 flow rate, but the vertexes are changed with the H_2 flow rate.

A single SOFC consists of two porous electrodes (anode and cathode, respectively) and an oxide ion conducting ceramic material as the solid electrolyte. Based on ECM circuit, we were able to obtain the best fitting result by employing five RQ elements as shown in Fig. 11, which suggests that the spectra are the result of a complex interplay between several competing reactions, including the reactions of electro-catalytic activation, ion conduction, mass transfer, and gas diffusion-coupled reactions with operation conditions [39]. Fig. 11 shows the proposed circuit model, in which an inductor and a resistor (R0) are connected with five R elements in series. R0 is from the ohmic resistance of the electrolyte, electrodes, and the connection wires; L is the inductance, which is attributed to the platinum current-voltage probes or the heating elements of the furnace used to heat up the sample. R elements correspond to the gas diffusion coupled with the charge transfer reaction and ionic transport, the oxygen surface exchange kinetics and oxygen ion diffusivity at cathode, and to the gas diffusion reaction [39], which will be clarified. Fig. 12 shows the change of R values with the over-potential at each temperature with 200 $ccmin^{-1}$ of 97% H_2 - 4.2% H_2O and 1,500 $ccmin^{-1}$ of air. R0 show similar values with the over-potential, and R1, R2, and R3 decrease with the over-potential. R4 decreases dramatically at 0.2 V of the over-potential, and R5 increase dramatically from 0.4 V of the over potential at 800 °C, from 0.5 V of the over-potential at 750 °C, and from 0.6 V of the over-potential at 700 °C. The mass transfer limitation occurs at lower over-potential and temperature, which results in higher impedance values. Figs. 14-17 show the fitted results with variation of the parameters. With increasing H_2O partial pressure, R1, R2, R3, and R5 decrease. R2, R3, R4, and R5 are reciprocally proportional to the H_2 partial pressure, and R4 is reciprocally proportional to the air partial pressure. In terms of H_2 flow rate, R2, R3, and R4 are proportional, while R5 is inversely proportional to H_2 flow rate. With the air flow rate, the polarization values are not changed.

The fitted polarizations results are shown in Table 1. Each of the proposed equivalent circuit elements is possibly associated with separate electrochemical events occurring in the fuel cell. It should be, however, noted that in analyzing impedance spectra using a fitting method, it is usually difficult to relate each of the elements to an actual physical event, since EIS is not a stand-alone test. An indirect, but effective way to glean further information on connecting the elements to an actual physical event is changing operation conditions and monitoring possible changes in R values. In this study, R0 is the ohmic resistance, and it is not changed with the change of fuel and oxidant supply. However, the R2 and R3 values are affected by the H_2 flow, which means that R2 and R3 are concerned with the anodic reactions. R5, as shown in Fig. 15 and 17, decreases dramatically with increasing H_2 flow rate, which means that R5 is related to the gas diffusion reaction in anode. R4 decreases with increasing air flow rate, which corresponds to the cathode mass limitation. It is difficult to clarify R1 with fuel and oxidants parameters, here. Leonide et al. also demonstrate an equivalent circuit of the anode-supported SOFC, which has five impedance elements connected in series by distribution of relaxation time [35,36,39.43]. They

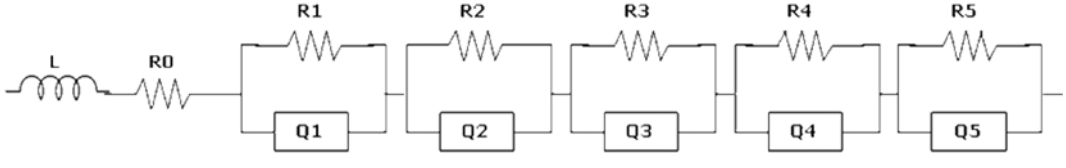

Fig. 11. Equivalent circuit.

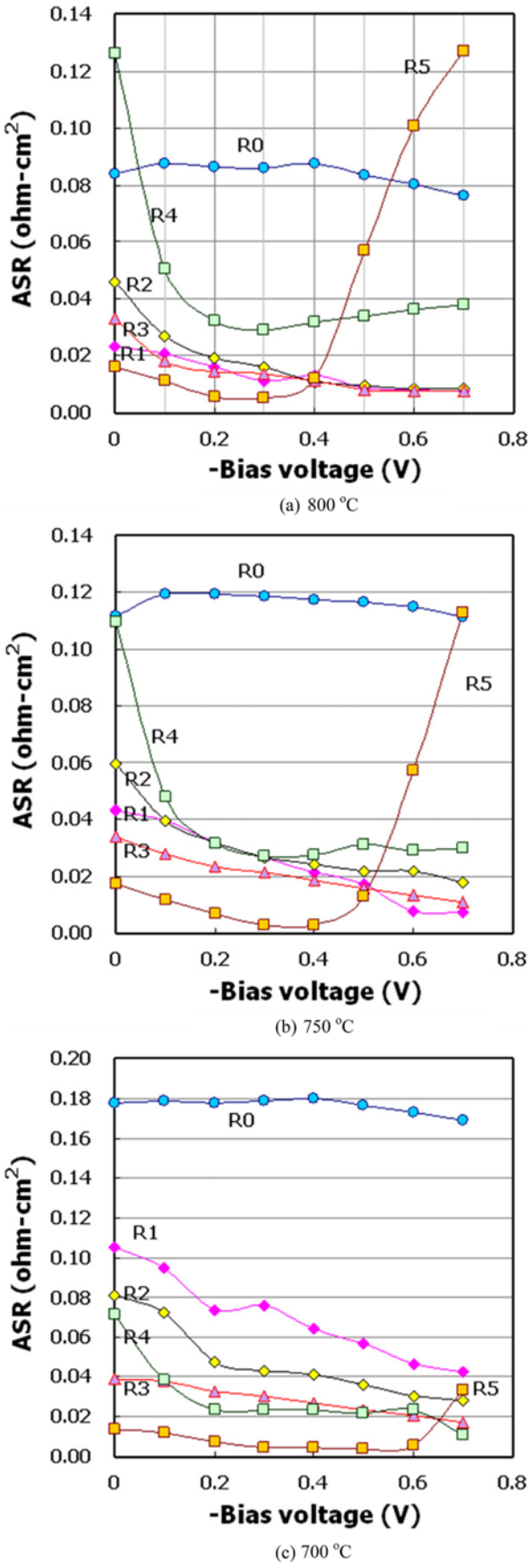

Fig. 12. Polarization elements with over-potential (a) 800 °C (b) 750 °C, and (c) 700 °C.

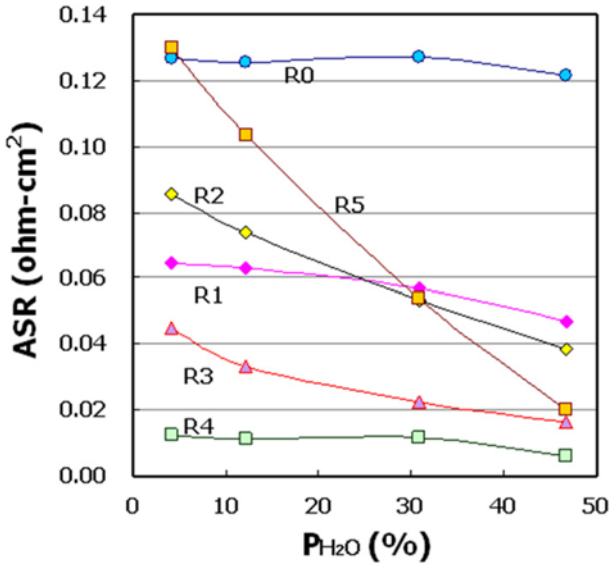

Fig. 13. Polarization elements with P_{H_2O}.

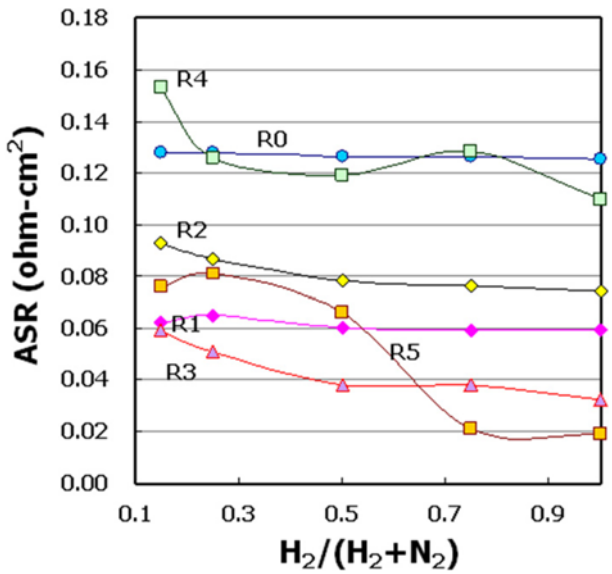

Fig. 14. Polarization elements with $H_2/(H_2+N_2)$.

report that the resistor R0 represents the ohmic resistance, while the resistors R1, R2, and R3 are associated with charge transfer reactions at the electrode, which include the gas diffusion coupled with the charge transfer reaction and ionic transport and the oxygen surface exchange kinetics and oxygen ion diffusion at cathode. R1, R2, and R3 respond sensitively to a disturbance in the high frequency range of 0.5-10 kHz. R4 and R5 are related to mass transfer at the electrode, responsive to a signal in the low frequency range of 1-100 Hz. Several recent studies also adopted a similar circuit model based on multiple impedance elements connected in series to describe measured impedance spectra [39,43].

In this work, five elements are suggested and tried to clarify the physical events on impedance responses by varying operation parameters. Two elements are concerned with anodic reaction of the gas diffusion coupled with the charge transfer reaction and ionic trans-

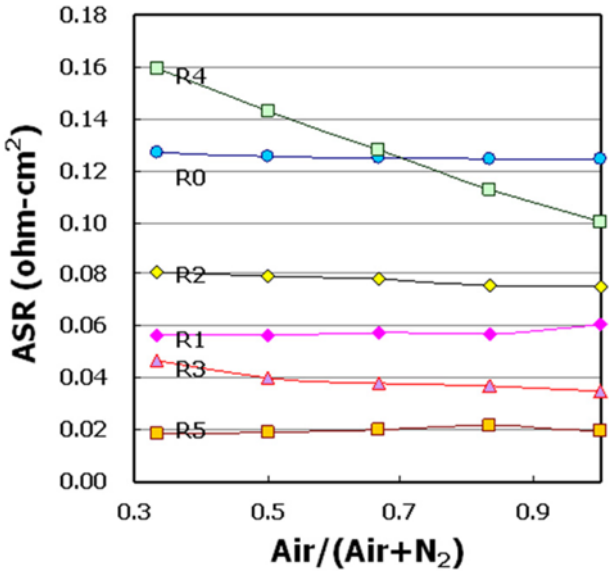

Fig. 15. Polarization elements with Air/(Air+N_2).

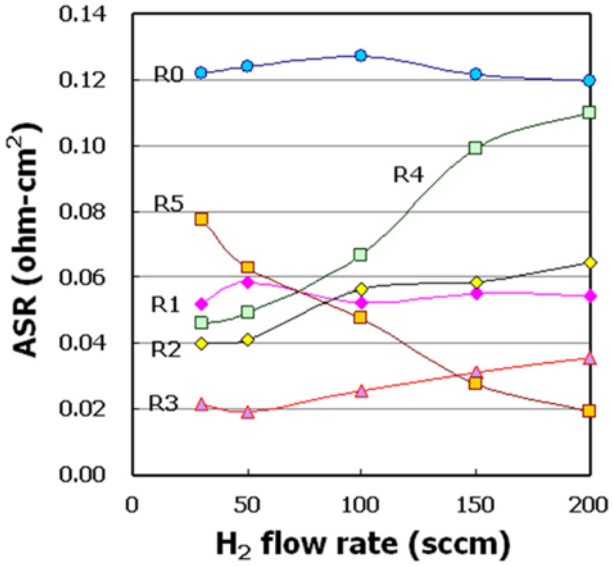

Fig. 16. Polarization elements with H_2 flow rate.

port. Another two elements are concerned with anode and cathode mass transfer reaction, respectively. However, one element is not easy to clarify. This work shows similar results in clarifying the elements of ECM, which means that the electrochemical diagnosis process comprises measuring, modeling with ECM, fitting, and interpretation is acceptable to use SOFC performance diagnosis [39]. The physical meaning of each element in this work may be very useful to find and develop the effects of materials and processes for SOFC, and the degradation mechanism can be analyzed to use the change of each element.

CONCLUSIONS

An anode-supported SOFC, consisting of an Ni-YSZ support/Ni-YSZ anode functional layer/YSA electrolyte/GDC interlayer/LSCF-GDC cathode, was prepared by a co-firing process and an aerosol deposition method. Anode-supported SOFCs were characterized as a function of operation conditions. In an air blowing system, the anode-supported SOFC shows an increment in fuel cell performance with increasing of H_2 partial pressure, increasing air partial pressure, and decreasing H_2O partial pressure. The air flow rate has no effect on impedance at 750 °C. The total impedance is not changed with the H_2 flow rate, but the vertexes are changed with the H_2 flow rate. To investigate the electrochemical response to impedances, the equivalent circuit is modeled and fitted by CNLS method. The five elements in equivalent circuit model are characterized. Two elements are concerned with the anodic reactions, while another two elements are related to the gas diffusion reaction in the electrode. One element among five is not easy to clarify. Each equivalent circuit element could show more than one reaction, and much work is needed to clarify the relationship among the electrochemical process, measurement variables, and their contribution to the impedance spectra of SOFCs. The results of this work may be used to develop the materials and process for SOFC by using the meaning of the elements in equivalent circuit model.

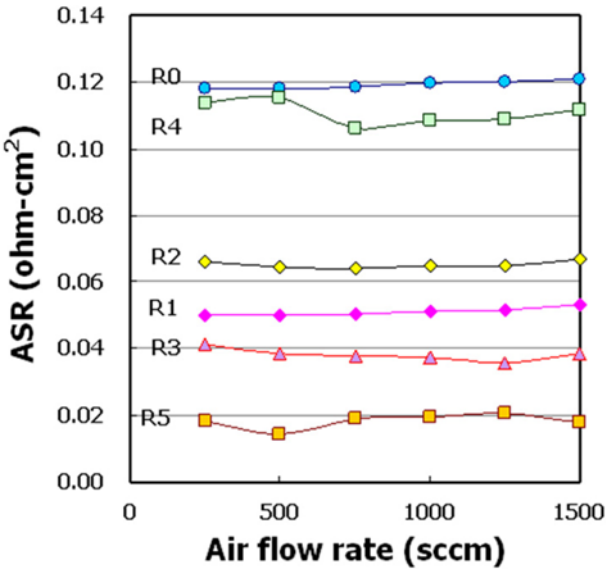

Fig. 17. Polarization elements with Air flow rate.

Table 1. Summary of fitted five elements with operation parameters

	Over-potential	P_{H_2O}	P_{O_2}	P_{H_2}	Air flow rate	H_2 flow rate
R0						
R1	↓	↓				
R2	↓	↓		↓		↑
R3	↓	↓		↓		↑
R4	↓		↓	↓		↑
R5	↓→↑	↓		↓		↑

ACKNOWLEDGEMENTS

This work was supported by the National Research Foundation (NRF) of Korea Grant funded by the Korean Government (MEST)

(NRF-2011-0009667).

REFERENCES

1. National Energy Technology Laboratory, *Fuel Cell Handbook seventh Ed*. DOE/NETL-2004/1206 (2004).
2. S. C. Singhal and K. Kendal, *High temperature solid oxide fuel cells fundamentals design and applications*, Elsevier Ltd., Oxford, England (2003).
3. J. Larminie and A. Dicks, *Fuel cell systems explained, second Ed.*, John Wiley & Sons, West Sussex, England (2003).
4. N. Q. Minh, *J. Am. Ceram. Soc*., **76**, 563 (1993).
5. S. Hui, J. Roller, S. Yick, X. Zhang, C. Decès-Petit, Y. Xie, R. Maric and D. Ghosh, *J. Power Sources*, **172**, 493 (2007).
6. F. Tietz, H. P. Buchkremer and D. Stöver, *Solid State Ionics*, **152-153**, 373 (2002).
7. S. C. Singhal and K. Kendall, *High Temperature Solid Oxide Fuel Cell*, Elsevier (2004).
8. F. Zhao and A. V. Virkar, *J. Power Sources*, **141**, 79 (2005).
9. H. Moon, S. D. Kim, S. H. Hyun and H. S. Kim, *Int. J. Hydrog. Energy*, **33**, 1758 (2008).
10. W. Bao, Q Chang and G. Meng, *J. Mem. Sci.*, **259**, 103 (2005).
11. K. C. Wincewicz and J. S. Cooper, *J. Power Sources*, **140**, 280 (2005).
12. V. A. C. Haanappel, J. Mertens and J. Malzbender, *J. Power Sources*, **171**, 789 (2007).
13. F. Zhao and A. V. Virkar, *J. Power Sources*, **141**, 79 (2005).
14. Y. Wang, M. E. Walter, K. Sabolsky and M. M. Seabaugh, *Solid State Ionics*, **177**, 1517 (2006).
15. K. Sato, H. Abea, T. Misono, K. Murata, T. Fukui and M. Naito, *J. Eur. Cera. Soc.*, **29**, 1119 (2009).
16. J. A. Kilner, R. A. De Souza and I. C. Fullarton, *Solid State Ionics*, **86-88**, 703 (1996).
17. J. Fleig, *Annu. Rev. Mater. Res.*, **33**, 361 (2003).
18. V. V. Srdic, R. P. Omorjan and J. Seidel, *Mater. Sci. Eng. B*, **116**, 119 (2005).
19. E. P. Murray, M. J. Sever and S. A. Barnett, *Solid State Ionics*, **148**, 27 (2002).
20. V. A. C. Haanappel, J. Mertens, D. Rutenbeck, C. Tropartz, W. Herzhof, D. Sebold and F. Tietz, *J. Power Sources*, **141**, 216 (2005).
21. J. H. Kim, Y. M. Park and H. Kim, *J. Power Sources*, **196**, 3544 (2011).
22. S. P. Jiang, *Solid State Ionics*, **146**, 1 (2002).
23. M. J. Jørgensen and M. Mogensen, *J. Electrochem. Soc.*, **148**, A433 (2001).
24. A. Mai, V. A. C. Haanappel, S. Uhlenbruck, F. Tietz and D. Stver, *Solid State Ionics*, **177**, 2103 (2006).
25. Y. Teraoka, H. M. Zhang, K. Kamoto and N. Yamazoe, *Mater. Res. Bull.*, **23**, 51 (1988).
26. J. Fleig, *J. Power Sources*, **105**, 228 (2002).
27. V. A. C. Haanappel, J. Mertens, D. Rutenbeck, C. Tropartz, W. W. Herzhof, D. Sebold and F. Tietz, *J. Power Sources*, **141**, 216 (2005).
28. S. B. Adler, J. A. Lane and B. C. H. Steele, *J. Electrochem. Soc.*, **143**, 3554 (1996).
29. J. A. Kilner, R. A. De Souza and I. C. Fullarton, *Solid State Ionics*, **86-88**, 703 (1996).
30. J. Fleig, *Annu. Rev. Mater. Res.*, **33**, 361 (2003).
31. V. Srdic, R. P. Omorjan and J. Seidel, *Mater. Sci. Eng. B.*, **116**, 119 (2005).
32. Q. Huanga, R. Hui, B. Wang and J. Zhang, *Electrochim. Acta*, **52**, 8144 (2007).
33. A. Leonide, B. Rüger, A. Weber, W. A. Meulenberg and E. Ivers-Tiffée, *J. Electrochem. Soc.*, **157**, B234 (2010).
34. V. Sonn, A. Leonide and E. Ivers-Tiffée, *J. Electrochem. Soc.*, **155**, B675 (2008).
35. A. Leonide, V. Sonn, A. Weber and E. Ivers-Tiffee, *ECS Transaction*, **7**(1), 521 (2007).
36. A. Leonide, V. Sonn, A. Weber and E. Ivers-Tiffee, *J. Electrochem. Soc.*, **155**(1), B36 (2007).
37. A. Weber, *International symposium on diagnostics tools fuel cell technologies* (2009).
38. H. Schichlein, A. C. Muller, M. Voigts, A. Krugel and E. Ivers-Tiffee, *J. Appl. Electrochem.*, **32**, 875 (2002).
39. V. Sonn, A. Leonide and Ivers-Tiffée, *ECS Transactions*, **7**(1), 1363 (2007).
40. A. Liliy, Y. X. Dunyushkin, S. B. Lu and Adlera, *J. Electrochem. Soc.*, **152**, A1668 (2005).
41. H. Kuboyama, T. Shoho and M. Matsunaga, *Electrochem. Proc.*, **97**, 404 (1997).
42. R. Barfod, M. Mogensen, T. Klemensø, A. Hagen, Y. L. Liu and P. V. Hendriksen, *J. Electrochem. Soc.*, **154**(4), B371 (2007).
43. C. Endler, A. Leonide, A. Weber, F. Tietz and E. Ivers-Tiffée, *J. Electrochem. Soc*., **157**(2), B292 (2010).